


Interaction between protoporphyrin IX and tryptophan silver nanoparticles

Carla R. Borges · Ricardo E. Samad ·
Karina de Oliveira Gonçalves · Daniel Perez Vieira ·
Lilia C. Courrol 

Received: 13 November 2017 / Accepted: 7 June 2018 / Published online: 19 June 2018
© Springer Nature B.V. 2018

Abstract Silver nanoparticles (AgNPs) have been intensively studied for several purposes including therapeutic applications in cancer. When prepared with tryptophan and photoreduction, silver nanoparticles (TrpAgNPs) become an alternative to conventional anticancer drugs. In this study, the anticancer activity of synthesized TrpAgNPs against MCF-7 breast cancer cells was evaluated, and the inhibitory concentration (IC₅₀) was found to be ~3.4 mg/mL. Since the protoporphyrin IX (PPIX) concentrations in tumor cells are elevated compared to normal cells, the PPIX-TrpAgNP interaction was studied to investigate if it could contribute for cell apoptosis. The investigation was performed using PPIX solution (0.9 µg/mL) with different TrpAgNP concentrations (from 0 to 13 mg/mL). PPIX was characterized by UV-Vis spectroscopy, steady-state and time-resolved fluorescence spectroscopy. The results have shown that the presence of spherical TrpAgNPs with 16-nm diameter quench the PPIX fluorescence intensity. This quenching is strongly dependent on the concentration of the TrpAgNPs, and it is caused by a combination of a static and a dynamic process. The

chemical binding leads to oxidation of tryptophan and formation of kynurenine, observed in the emission spectra around 470 nm. The strong reduction of the PPIX fluorescence decay lifetime with nanoparticle increasing concentration confirms the quenching processes due to charge transfer from the excited PPIX states to the resonant silver states. The present study confirms the anticancer activity of TrpAgNPs on the human breast cancer cell line (MCF-7) *in vitro* and indicates that PPIX-AgNP interaction could contribute with MCF-7 apoptosis.

Keywords Silver nanoparticles · Porphyrin · Kynurenine · Cancer · Theranostic · Nanobiomedicine

Introduction

Cancer is a multifactorial disease that has uncontrolled growth and spread of anomalous cells due to a combination of genetic, external, internal, and environmental factors (Weis et al. 2005; Thompson et al. 2008). Cancer treatments comprise surgery, chemotherapy, and radiation, immune, hormonal, photodynamic, targeted, and particle therapies (Zhang et al. 2016; Giantsoudi et al. 2017). Some of these therapeutic treatments induce severe cytotoxicity to normal cells (Yen et al. 2009; Han and Chen 2013), and new treatments have been proposed trying to improve the cure rate and reduce the side effects (Sanna et al. 2014; Giantsoudi et al. 2017). Much interest has grown up around the use of porphyrins, which have a high tumor-targeting ability and

C. R. Borges · K. de Oliveira Gonçalves · L. C. Courrol (✉)
Departamento de Física, Universidade Federal de São Paulo,
Diadema, SP, Brazil
e-mail: lccourrol@gmail.com

R. E. Samad
Centro de Lasers e Aplicações, IPEN-CNEN/SP, São Paulo, SP,
Brazil

D. P. Vieira
Centro de Biotecnologia, IPEN-CNEN/SP, São Paulo, SP, Brazil

phototoxicity, and were linked to various anticancer agents to selectively transport and destroy tumor tissues (Zhou et al. 2016). Particularly, the use of protoporphyrin IX (PPIX) has received attention as a potential agent for cancer diagnostic and therapy (Yang et al. 2015; Huntosova et al. 2016; Blanco et al. 2015; Bae et al. 2016). Besides accumulating more in tumor tissues than in normal ones (de Oliveira Silva et al. 2011), PPIX has potent photosensitizing capabilities that can be exploited in photodynamic therapy (PDT) (Yang et al. 2015). PPIX is also a photo diagnostic agent capable to identify and delimit the margins of tumors, and its fluorescence properties can be used to monitor changes during PDT (Namikawa et al. 2015; Blanco et al. 2015; Bae et al. 2016). PPIX exhibits maximum light absorption (the Soret peak) at 405-nm and dual-emission peaks at 635 and 705 nm (Silva et al. 2013).

In the same way, as with PPIX, silver nanoparticles (AgNPs) have been extensively studied due to their therapeutic applications in cancer (Zhang et al. 2016; Satapathy et al. 2014). AgNPs can induce cell death through various processes, including reactive oxygen species (ROS) generation and DNA damage, among others (Zhang et al. 2016). AgNPs are one of the most commercialized nanoparticles worldwide, and are used in various fields due to their optical, electrical and thermal properties (Desai et al. 2012). Recently, AgNPs have become of extreme interest in biomedical applications because of their antibacterial, antifungal, antiviral, antiinflammatory, and anticancer activities (Sweet et al. 2012; Rai et al. 2012). To successfully use silver nanoparticles in various applications, their structural features such as size, shape, composition, and surface chemistry must be considered. To synthesize AgNPs, physical, chemical, and biological methods have been applied (Bastus et al. 2014; Courrol et al. 2007; Durán et al. 2015; Gottesman et al. 2011; Horikoshi et al. 2010; Kamat 2002). Although chemical and physical approaches have a high degree of controlling the shape and size of the AgNPs during their synthesis, the biological/environmental toxicity and the high cost of equipment are the main disadvantages of these methods. The biocompatible silver nanoparticles produced with tryptophan (TrpAgNPs) and a green method demonstrated potential antibacterial activity (Tomita et al. 2014), and have requirements as potent anticancer candidate. Studies demonstrated that the tryptophan nanoparticles can reduce potential hepatotoxicity and nephrotoxicity (Shmarakov et al. 2014).

Several studies reported that silver nanoparticles mediated production of reactive oxygen species (ROS) plays an important role in cytotoxicity (Yen et al. 2009; Xin et al. 2016). Many studies have suggested that AgNPs are responsible for biochemical and molecular changes related to genotoxicity in cultured cells such as DNA breakage (Xin et al. 2016; Satapathy et al. 2013). In this paper, the cytotoxicity effects of TrpAgNPs against MCF-7 breast cancer cells were studied. To obtain essential knowledge about the interaction between PPIX molecules and TrpAgNPs, the present study performed a close analysis of the PPIX fluorescence behavior when surrounded by different concentrations of TrpAgNPs. The investigation was performed using PPIX solutions with different TrpAgNP concentrations (from 0 to 13 mg/mL), to evaluate the potential implication of TrpAgNPs and PPIX in apoptosis.

Materials and methods

The PPIX solutions fluorescence behaviors were investigated in absence and in the presence of variable concentrations of TrpAgNPs. The details of the experimental steps are given below.

Silver nanoparticles were synthesized as described previously (de Matos and Courrol 2017); in brief, 62 mg of tryptophan (Vetec) and 8 mg of AgNO₃ (Sigma) were added to 100 mL of Milli-Q water. This solution was stirred in a vortex mixer for 5 min. Ten-milliliter volume of the prepared solution was illuminated with a 300-W xenon lamp (Cermex, Excelitas Technology) for 5 min. The Xe lamp was positioned 10 cm away from the recipient containing the solution, and the illuminated region covered exactly the recipient diameter, with a 3.6-W/cm² estimated intensity. The final solution pH after Xe illumination was ~6.95.

The TrpAgNP concentration ($\sim 1.27 \times 10^{-6}$ M) was calculated using the extinction coefficient (ϵ) for silver nanoparticles in water and the Mie theory-based power law equation, $\epsilon = Bd\gamma$, where $B = 2.3 \times 10^5 \text{ M}^{-1} \text{ cm}^{-1}$ and $\gamma = 3.48$ for $d \leq 38 \text{ nm}$ (Navarro and Werts 2013). The average diameter (d) of the silver nanoparticles was ~16 nm.

To obtain the silver concentration in mg/ml, it was initially considered that the nanoparticles have an 8-nm radius (average value) and the same density as bulk silver (10.49 g/cm³), giving the mass of a nanoparticle. This nanoparticle mass was multiplied by their molar

concentration, providing the start solution concentration (17.2 mg/ml). Subsequent dilutions were considered for the concentration-dependent studies.

Cell culture

MCF-7 cells (8×10^3 /well) were placed in 96-well plates and incubated overnight at 37 °C with 5% CO₂. TrpAgNPs at increasing concentration 0–9 mg/mL (5 μL in 95-μL RPMI, 10 μL in 90-μL RPMI, 20 μL in 80-μL RPMI, 30 μL in 70-μL RPMI, 40 μL in 60-μL RPMI, and 50 μL in 50-μL RPMI) were added to the cells and incubated at 37 °C with 5% CO₂. After 24 h, the cells were washed with PBS buffer and the culture medium RPMI-1640 was added to the cells. The cells were then incubated for growth for 24 h to express damage. MTS(3-(4,5-dimethylthiazol-2-yl)-5-(3-carboxymethoxyphenyl)-2-(4 sulfophenyl)-2H tetrazolium) was added to each well and incubated for 2 h. In this procedure, the cells were incubated with fresh medium containing MTS reagent for 2 h before measurements at 490 nm. The effect of the nanoparticles on cell proliferation was expressed as percentage of inhibition of cell growth relative to the control. The percentage of cell survival was calculated after background absorbance correction and blank absorbance subtraction as follows: % cell viability = 100 × experimental well absorbance / untreated control well absorbance.

PPIX solutions

A PPIX solution with 56 μg/mL concentration was prepared solving protoporphyrin IX (Sigma CAS number 553-12-8) in acetone P.A. (Synth).

TrpAgNP-PPIX solutions

To study the interaction between PPIX and TrpAgNPs, 300 μL of the PPIX solution was added to 1 mL of the TrpAgNPs solutions at concentrations from 0 to 13 mg/mL. The final PPIX concentration was 0.9 μg/mL.

PPIX extraction from MCF7

MCF7 cells were incubated with aminolevulinic acid (ALA) 30 nM (40 μL of ALA in 60-μL serum-free RPMI-1640) or 100 μL of culture medium for 24 h. Then, the cells were washed several times with

phosphate-buffered saline (PBS) (pH = 7.2–7.6). The ALA-free cells were suspended in 500 μL media, and the contents of each well were collected and added to tubes containing 3 volumes of acetone. These solutions were then centrifuged for 15 min at 4000 rpm, and the supernatants were analyzed in a 3 Fluorolog Jobin Yvon fluorimeter. The samples were excited at 405 nm, and the emission spectra were measured between 415 and 785 nm. The excitation bandwidth was 5 nm.

Optical measurements

The absorption spectra of the solutions were measured in the range 300–800 nm with a Shimadzu MultiSpec-1500 spectrophotometer, at room temperature. The solutions were poured into a 1-cm optical path quartz cuvette.

The fluorescence measurements of prepared PPIX with TrpAgNP solutions were performed using a RF-5301 (Shimadzu Scientific Instruments) fluorimeter. The sample fluorescence spectra were obtained for wavelengths between 420 and 780 nm, under excitation at 400 nm. All measurements were carried out at room temperature using a quartz cuvette with four polished faces and 1-mm optical path.

The PPIX fluorescence lifetimes were obtained using a system composed by a pulsed diode laser (PDL 800-B, PicoQuant) generating 45-ps pulses, centered at 403 nm, in an 8-MHz repetition rate pulse train, and 0.1 mW of average power. The detection was performed using a photomultiplier (Hamamatsu PMA 182-PM) and a RG610 long-pass colored glass filter. A reflective neutral density filter ND30A (ThorLabs) was used to reduce the background noise. The obtained data was processed using PicoQuant PicoHarp 300 (TCSPC system connected to a PC through a USB 2.0 interface) and analyzed using Mathematica® 11 software.

The normalized intensity emission profiles, $I(t)$, were fitted by a triple-exponential decay curve:

$$I(t) = bg + A_1 \exp\left(-\frac{t}{\tau_1}\right) + A_2 \exp\left(-\frac{t}{\tau_2}\right) + A_3 \exp\left(-\frac{t}{\tau_3}\right) \quad (1)$$

where bg is the background noise and the τ_i and A_i are the lifetime components and their relative weights (amplitudes), respectively.

The amplitude-weighted lifetime τ_{mean} was calculated according to:

$$\tau_{\text{mean}} = \frac{\sum A_i \tau_i^2}{\sum A_i \tau_i} \quad (2)$$

Results

Figure 1 shows the UV-Vis spectra and a TEM image of the synthesized TrpAgNPs. This figure indicates the surface plasmon resonance (SPR) band around 440 nm, and the differential particle size histogram that shows particles with sizes ranging from 8 to 25 nm. For the obtained nanoparticles, the zeta potential value was -31.8 mV and the polydispersity index was 0.512.

Cytotoxic potential of TrpAgNPs against breast cancer cells in vitro

The in vitro anticancer activity of TrpAgNPs was studied using MTS assay at different concentrations, and the inhibitory effect (IC₅₀) in MCF-7 cancer cell lines was determined by plotting the chart of different concentrations versus percentage (%) of cell viability by a dose-response curve shown in Fig. 2. As the concentration increases, there is a decrease in the percentage of cell viability, demonstrating a direct dose-dependent

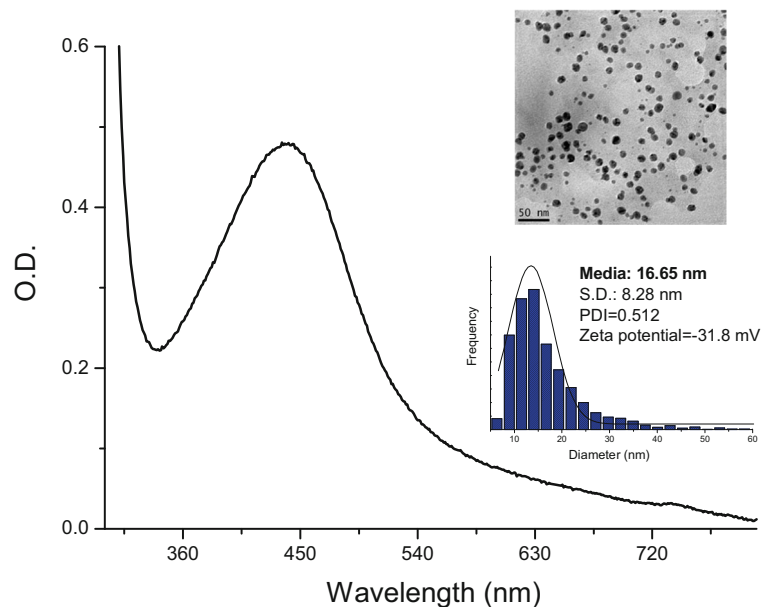
relationship and an increase in cell death. The results confirmed that the absorbance of the cell line decreased while increasing the concentration because of the higher toxicity against the cancer cells. The IC₅₀ value for this reduction in percentage of cell viability of MCF-7 cell lines was found to be ~ 3.4 mg/mL. Results were statistically compared (ANOVA) to negative (control cells, NaCl 0.9%) and positive (latex powder suspension 0.5 g/L in culture media, 24 h), showing $p \leq 0.0001$ for concentrations > 5 mg/mL compared to the control group.

TrpAgNP-PPIX interaction

Figure 3a shows the excitation (emission at $\lambda_{\text{em}} = 631$ nm) and fluorescence (excitation at $\lambda_{\text{exc}} = 400$ nm) spectra of the PPIX solution. The PPIX has maximum light absorption (the Soret peak) at 400 nm. The fluorescence spectrum presents a band around 455 nm due to the acetone Raman when excited at 400 nm, and dual-emission peaks at ~ 631 and ~ 700 nm.

The fluorescence spectra obtained for PPIX extracted from MCF7 cells without and with aminolevulinic acid incubation are shown in Fig. 3b. An ALA-induced PpIX emission peak at 630 nm with a shoulder at 700 nm can be observed in this figure. The PPIX emission was not identified in the spectrum without ALA incubation since the emission intensity is out of the detection limit. It was

Fig. 1 Optical absorption spectra of TrpAgNPs, size distribution, and TEM image



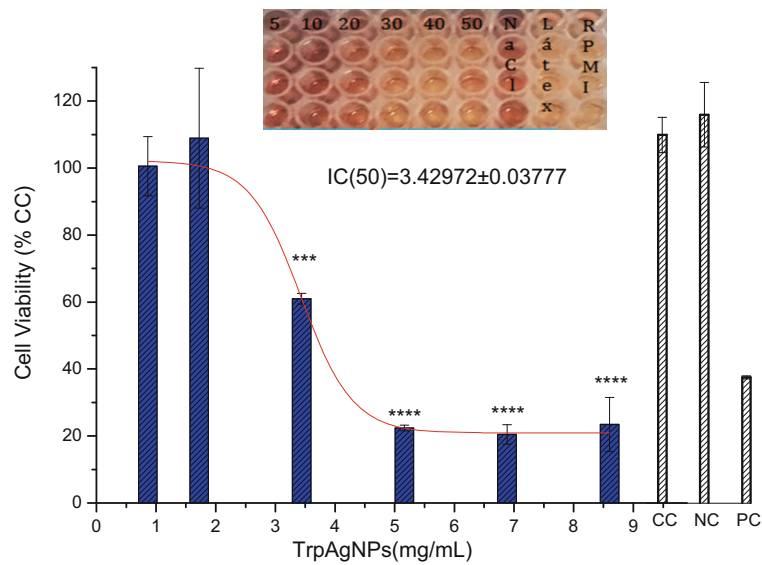


Fig. 2 Cytotoxicity assay. Assessment of TrpAgNPs induced cell death in MCF-7 breast cancer cell. The cells were treated with a range of concentration of TrpAgNPs 0–9 mg/mL (5 μ L in 95- μ L RPMI, 10 μ L in 90- μ L RPMI, 20 μ L in 80- μ L RPMI, 30 μ L in 70- μ L RPMI, 40 μ L in 60- μ L RPMI, and 50 μ L in 50- μ L RPMI) and incubated for 24 h. The percent of cell viability was determined by MTS assay. The values are averages of triplicate assays

in three experiments: CC—control group (untreated cells), PC—positive control (latex powder suspension, 0.5 g/L), and NC—negative control (NaCl 0.9%). Asterisks denote examples of statistical significance in comparison with untreated cell controls using a one-way ANOVA by Tukey’s mean comparison (** $p < 0.001$ and **** $p < 0.0001$)

not possible to demonstrate that the PPIX-TrpAgNP interaction with PPIX extracted from cells, and for this reason, a PPIX solution with $\sim 0.9 \mu\text{g/mL}$, which is on the same order of magnitude as found in tumor areas, was prepared.

PPIX emission spectra in the presence of variable TrpAgNP concentrations are presented in Fig. 4a, showing that the increase in TrpAgNP concentration results

in a decrease of the PPIX emission band and a growth in a band around 470 nm. This band is attributed to the kynurenine (Kyn) (Lesniak et al. 2013), which is a product of the tryptophan oxidation.

Figure 4b shows the fluorescence suppression (F_0/F fluorescence ratio, where F_0 and F are the PPIX intensity at 631 nm in the absence and presence of the silver nanoparticles, respectively), plotted as a function of the

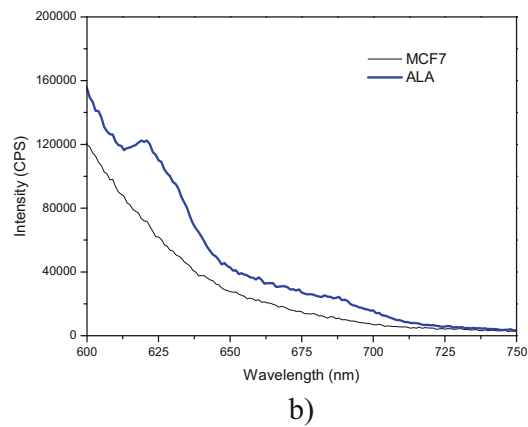
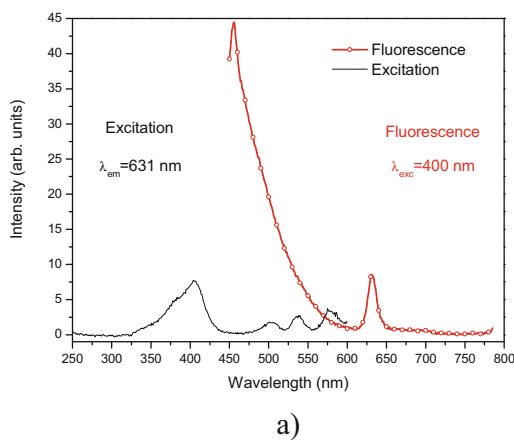


Fig. 3 a PPIX solution excitation and fluorescence spectra. The fluorescence spectrum was obtained by excitation at 400 nm. Excitation spectrum was obtained fixing emission at 631 nm. **b**

Fluorescence spectra of PPIX extracted from MCF7 cells without and with aminolevulinic acid incubation

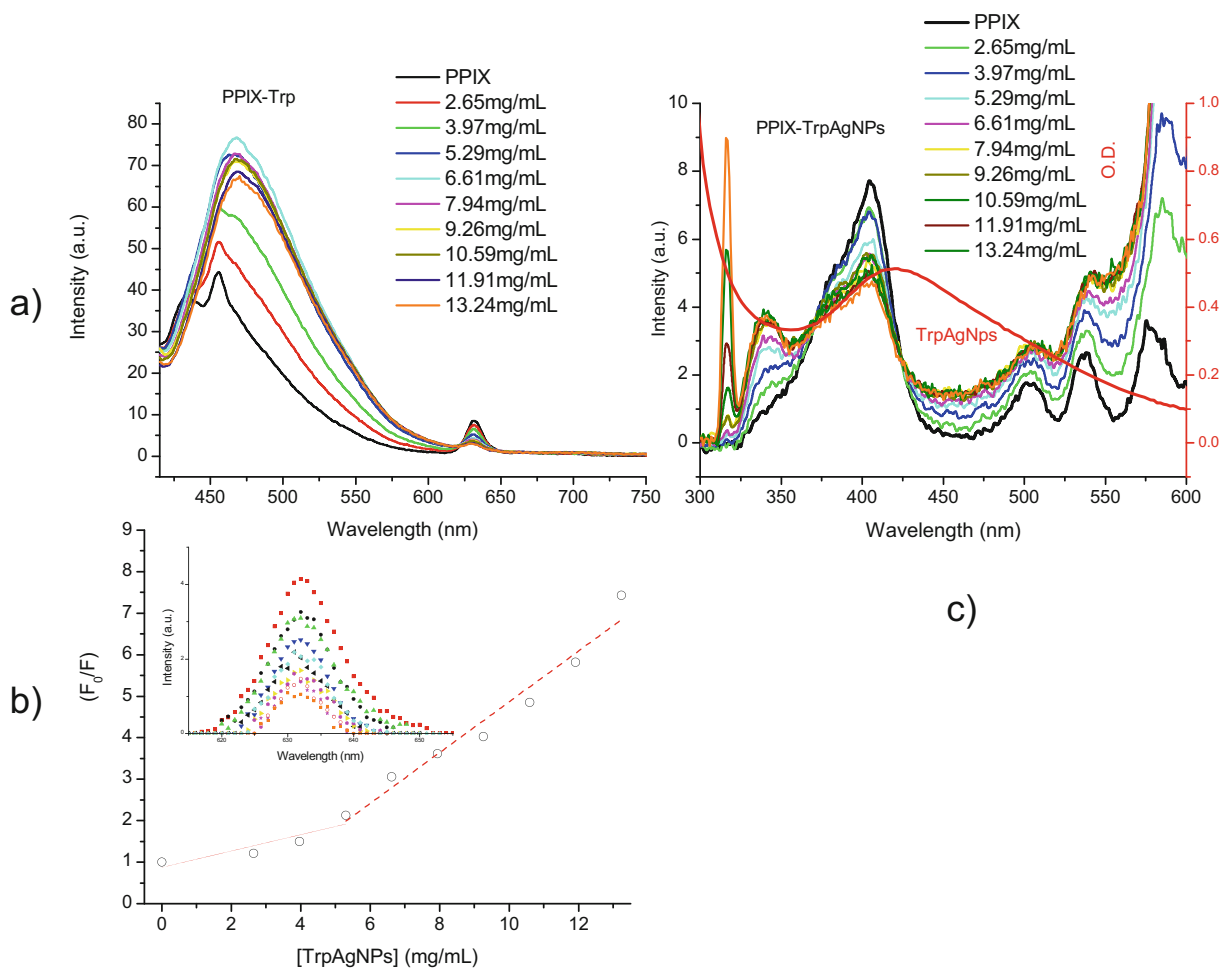


Fig. 4 **a** PPIX-TrpAgNP emission spectra obtained with excitation at 400 nm. **b** Stern–Volmer fit curve for PPIX-TrpAgNPs. The inset figure shows the emission spectra in the range 610–660 nm

after baseline subtraction. **c** Excitation spectra ($E_m = 631$ nm) of PPIX-TrpAgNPs. *right axis* TrpAgNP absorption band

TrpAgNP concentration. The experimental points were obtained after baseline subtraction of the PPIX emission band around 631 nm (inset in Fig. 4b).

A typical Stern–Volmer plot (F_0/F) versus concentration provides the kinetic efficiency of the fluorescence quenching. Stern–Volmer equation is:

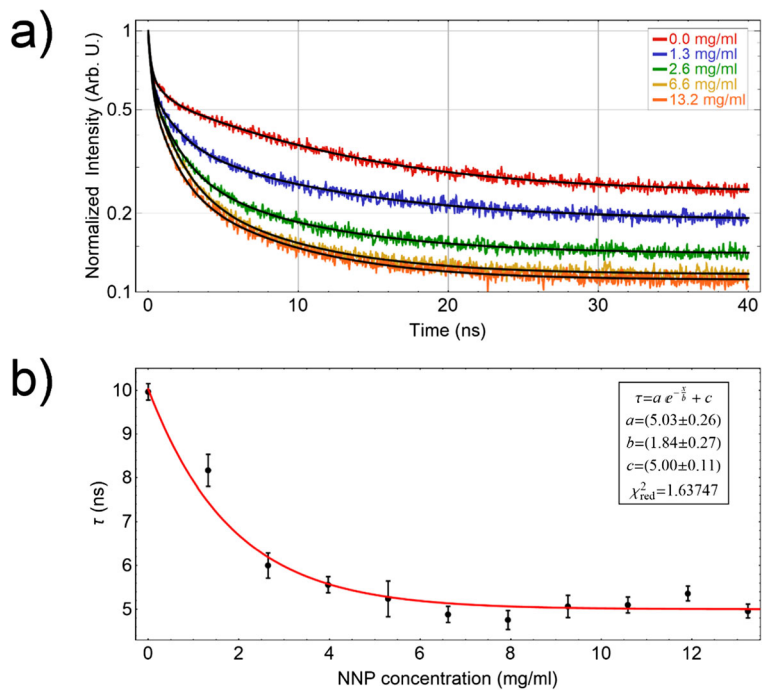
$$\frac{F_0}{F} = 1 + k_q \tau_0 [Q] = 1 + K_{SV} [Q] \quad (3)$$

where F_0 and F are the fluorescence emission intensities in the absence and presence of the quencher, respectively; k_q is the bimolecular quenching rate constant; τ_0 is the lifetime of the fluorophore in the absence of quencher; K_{SV} is the Stern–Volmer constant (which is a measure of the efficiency of quenching), and $[Q]$ is the quencher concentration. It is also used to differentiate

the mechanism of the fluorescence quenching. Formation of the ground state complex between fluorophore and quencher involves static quenching while the dynamic quenching originates from collisions.

The results shown in Fig. 4b indicate a deviation from linearity in Stern–Volmer plot toward upward curvature at higher concentrations (> 5.3 mg/mL) of TrpAgNPs. Figure 4c shows the effect in the excitation spectra (ground-state absorption) in the presence of TrpAgNPs. These spectra were obtained fixing emission at 631 nm. The TrpAgNP surface plasmon band is shown in the same figure (right axis in red). The SPR band of TrpAgNPs appears damped in the presence of PPIX. The absorption band around 350 nm is compatible with kynurenine absorption band. The other changes observed in the excitation spectra are attributed to

Fig. 5 **a** Fluorescence decays for solutions containing different TrpAgNP concentrations. **b** Amplitude-weighted lifetime as a function of TrpAgNP concentration



charge-transfer bands for donor (PPIX)–acceptor systems (Imahori et al. 2005).

PPIX fluorescence lifetime

The PPIX fluorescence decays for different nanoparticle concentrations were measured, and the results are shown in Fig. 5a. The decay curves were fitted by triple-exponential decay curves (Eq. 1).

The amplitude weighted lifetimes, τ_{mean} , and their components obtained from the fittings by Eq. 2, for the PPIX with the TrpAgNPs, are shown in Fig. 5b. By the fit parameters shown in Table 1, it is possible to observe that τ_1 is constant, and τ_2 and τ_3 decrease with increasing nanoparticle concentration; the PPIX emission amplitude-weighted lifetime starts at 10 ns for a solution without nanoparticles, and decreases with the addition of nanoparticles, saturating at 5 ns for nanoparticle concentrations higher than 5.3 mg/mL.

Table 1 Fit parameters obtained for PPIX

Nanoparticle concentration (mg/mL)	τ_1 (ns)	τ_2 (ns)	τ_3 (ns)	τ_{mean} (ns)
0	0.17 ± 0.02	10.41 ± 0.18	0.84 ± 0.13	9.96 ± 0.19
1.32	0.22 ± 0.01	9.90 ± 0.38	1.66 ± 0.10	8.17 ± 0.37
2.65	0.21 ± 0.01	8.29 ± 0.33	1.69 ± 0.06	6.00 ± 0.29
3.97	0.21 ± 0.01	8.00 ± 0.22	1.58 ± 0.04	5.56 ± 0.18
5.29	0.21 ± 0.01	7.71 ± 0.49	1.61 ± 0.08	5.24 ± 0.41
6.61	0.21 ± 0.01	7.01 ± 0.22	1.50 ± 0.04	4.88 ± 0.19
7.94	0.19 ± 0.01	6.90 ± 0.25	1.45 ± 0.05	4.75 ± 0.22
9.26	0.23 ± 0.01	7.47 ± 0.30	1.53 ± 0.05	5.06 ± 0.25
10.59	0.22 ± 0.01	7.08 ± 0.20	1.34 ± 0.05	5.10 ± 0.18
11.91	0.21 ± 0.01	7.30 ± 0.19	1.36 ± 0.04	5.36 ± 0.17
13.24	0.201 ± 0.01	6.78 ± 0.18	1.29 ± 0.04	4.96 ± 0.16

Discussion

TrpAgNPs present interesting properties as size distribution, shape, particle morphology, and particle composition. These properties are attractive for therapeutic applications in cancer, considering that the use of tryptophan attenuates the potential hepatotoxicity and nephrotoxicity of nanoparticles (Shmarakov et al. 2014).

Various types of cell lines can react differently after incubation with nanoparticles. Biochemical and genetic changes and the oxidative stress may be the main factors causing cytotoxicity (Tang et al. 2015). The present study confirms the anticancer activity of TrpAgNPs on human breast cancer cell line (MCF-7) *in vitro*. The IC₅₀ analysis confirmed that the TrpAgNPs produced a significant cytotoxic effect (Baskaran et al. 2017). This result is very important considering that multi-drug resistance of breast cancer is a major obstacle in chemotherapy of cancer treatments (Feuerstein et al. 2011).

Endocytosis and passive diffusion have been proposed as mechanisms for the uptake into cells of NPs (Feliu et al. 2016; Shang et al. 2014; Kettler et al. 2014). Particles can cross the membrane only if they are at most 10 to 30 nm in size. By a process called facilitated diffusion, the water-soluble nanoparticles pass through the membrane via pores. Larger particles are typically encapsulated in vesicles and selectively transported into the cells by the endocytosis mechanism (Shang et al. 2014). In most cells, internalization occurs via pinocytosis. The size, as well as the coating, can also influence the subcellular distribution of the internalized NPs. Studies demonstrate that uptake into cells depends strongly on NP size, with an optimum incorporation at an NP diameter of approximately 50 nm (Kettler et al. 2014). Increased charge, either positive or negative, favors uptake in cells and an increase in the absolute zeta potential usually leads to increased NP uptake in comparison with less charged NPs of the same size (Kettler et al. 2014).

In our experiment, MCF-7 cells were exposed to TrpAgNP water solutions. Some important properties of the TrpAgNPs should be considered: (1) size is around 16 nm and both endocytosis and passive internalization are possible; (2) TrpAgNPs present (–COOH) functional groups that add a negative charge to nanoparticles and favors uptake, and (3) zeta potential value that is > -30 mV, which supports NP uptake.

Several *in vitro* models suggest that ROS-mediated toxicity is more pronounced and causes cellular and biochemical alteration in the cells (Austin et al. 2015;

Valko et al. 2006; Song et al. 2011). Austin et al. suggested that the increased AgNP cytotoxicity is due to their ability to generate increased concentrations of ROS, which leads to disruption in various other cellular functions (i.e., DNA synthesis, mitochondrial activity, cell cycle progression) (Austin et al. 2015). Furthermore, cytotoxicity is shown to increase dramatically with the nanoparticle proximity and localization at the nucleus. Suresh et al. (2012) investigated the toxicity of AgNPs in epithelial cells. They concluded that toxicity depends not only on surface coating but also on the cell type.

It is known that PPIX preferentially accumulates in human breast cancer MCF-7 (Li et al. 2014; Millon et al. 2010), so the possible interaction between TrpAgNPs and PPIX was studied.

The relative change in PPIX fluorescence intensity could discriminate breast cancer from normal mammary epithelial cells (Millon et al. 2010). It is hard to estimate the value of PPIX concentration in tumor areas. This value depends on the tumor stage, size, and tumor type. Sunar et al. (2013) quantified the protoporphyrin IX (PpIX) distribution induced by topical and intratumoral administration of the prodrug ALA in basal and squamous cell carcinoma murine models by using a spatial frequency domain imaging. The absolute PpIX concentrations estimated had a maximum value of ~ 0.5 $\mu\text{g/mL}$. Concentrations of PPIX in normal cells have been found to be low, whereas they are high in tumor cells since the enzyme ferrochelatase, which converts protoporphyrin IX to heme, has been found to be reduced in cancerous cells (Feuerstein et al. 2011). In MCF 7 cells, PPIX is mostly accumulated in the mitochondria according to Li et al. (2014).

In our experiment, the hypothesis, not demonstrated experimentally, is that TrpAgNP size, charge, and stability favor the internalization in MCF-7 cells via pinocytosis. By this process, the silver nanoparticles can enter in the cytosol within pinosomes. The pinosomes can then fuse with lysosomes, where the TrpAgNPs in an acidic medium could be catabolized forming tryptophan and Ag ions, which would produce increments of reactive oxygen species. The kynurenine pathway could be initiated simultaneously to the formation of PPIX-Ag complexes that would bind to DNA and cause damage via oxidative mechanisms, culminating in cell apoptosis.

The quantification of PPIX in MCF7 cells without 5-ALA was not possible by fluorescence, as shown in Fig.

3b, which makes the demonstration of quenching in live cells difficult. Certainly, this process could be demonstrated *in vivo*, but fluorescence emissions contain background contributions from excitation light leakage, autofluorescence, and photoproducts which may alter the lower limit of sensitivity to PPIX (Mansfield et al. 2005). A series of processing methods and techniques as hyperspectral imaging (Bravo et al. 2017) or special frequency domain imaging (Sunar et al. 2013) could demonstrate the PPIX-TrpAgNP interaction *in vivo*.

The interaction between PPIX molecules and TrpAgNPs was investigated by analyzing the PPIX fluorescence properties to understand the nature of this interaction as well as evaluate the potential impacts in cancer therapy. The investigation was performed using PPIX solutions (~ 0.9 $\mu\text{g/mL}$) with different TrpAgNP concentrations (from 0 to 13 mg/mL). With increasing amounts of TrpAgNPs, the probability of TrpAgNP-PPIX interaction increases accordingly.

The results presented in Fig. 4, for some TrpAgNP concentrations, show that a quenching of the fluorescence intensity occurs, and it is TrpAgNP content-dependent.

Deviation from linearity in the Stern–Volmer plot (Fig. 4b), toward upward curvature at higher concentrations (> 5.3 mg/mL) of TrpAgNPs favors static quenching (dotted line), while dynamic quenching (the straight line) exists at lower concentrations. With increase in the concentration of TrpAgNPs (> 5.3 mg/mL), the interaction between TrpAgNPs and PPIX becomes multifarious. Similar quenching behavior was reported by Devi et al. (2014) upon the interaction of AgNPs with hemoglobin, where the upward curvature in Stern–Volmer plot indicates dynamic quenching at low concentration and static quenching at high concentration of AgNPs.

The surface plasmon band of TrpAgNPs appears damped in the presence of PPIX as shown in Fig. 4c. Surface plasmon band dampening upon chemisorption of various species has been previously observed (Murphy et al. 2011; Linnert et al. 1993). Chemisorption often leads to the formation of complexes capable of charge-transfer transitions.

As presented in Fig. 5b, the average lifetime indicates that the addition of TrpAgNPs in the PPIX reduces the fluorescence lifetime of the samples. The lifetime components originate from different species: τ_1 is attributed to the acetone fluorescence due to its constancy (the PPIX solvent in this experiment was acetone; in the

in vivo interaction, the τ_1 component should be attributed to the cellular medium); τ_2 is attributed to the PPIX, which is strongly modified by the nanoparticles presence; and τ_3 is a fast decay also modified by the nanoparticle presence.

We propose that the strong reduction of the fluorescence decay time attributed to the PPIX (τ_2 in Table 1) in the presence on silver nanoparticles is associated to the enhanced quenching process due to charge transfer from the excited PPIX states to resonant silver states. During the interaction between the PPIX and the TrpAgNPs, the nanoparticle surface plasmon is dampened by chemisorbed PPIX molecules, leading to the formation of complexes capable of charge-transfer transitions (Murphy et al. 2011). The PPIX from which the charge is transferred is the electron donor and the TrpAgNP is the electron acceptor. As more TrpAgNP surface area/PPIX molecule is made available in the solution, a higher percentage of PPIX molecules can directly interact with the nanoparticles and participate in chemical binding. The residual bleaching is attributed to charged products, which becomes stabilized by the solvent medium. The oxidation of tryptophan and formation of Kynurenine (Mukha et al. 2016) was observed. This must occur because part of the PPIX molecules transfer energy to the ground state oxygen generating reactive oxygen species. The singlet oxygen generated in this process can oxidize the molecules of tryptophan generating kynurenine. With the increase of total TrpAgNP concentration, the PPIX quenching increases. The quenching process increases up to a concentration around 5.3 mg/mL , when it saturates.

For concentrations higher than 5.3 mg/mL , the kynurenine band decreases. The increase of nanoparticles concentration in the solution reduces the concentration of free PPIX through interaction with their surfaces. Probably this process reflects a limitation of TrpAgNP surface area/PPIX molecule.

Wide-scale and vigorous studies are still needed to better assess the risks and hazards, associated with the use of TrpAgNPs in the pursuit of medical advancements.

Conclusions

The anticancer activity of synthesized TrpAgNPs against MCF-7 breast cancer cells was evaluated and the inhibitory concentration (IC50) was found to be

3.4 mg/mL and confirmed the anticancer activity of TrpAgNPs on human breast cancer cell line (MCF-7) in vitro. The most probable mechanism of TrpAgNP-induced toxicity is oxidative stress. Considering the increased amount of PPIX in the MCF7 cytoplasm, the interaction between TrpAgNPs and PPIX was studied. We demonstrated that silver nanoparticles quench the fluorescence of PPIX, leading to a reduction in emission lifetime. An energy transfer process from excited PPIX to the ground state oxygen molecules ($^3\text{O}_2$) give rise to $^1\text{O}_2$ molecules that promote tryptophan oxidation and formation of kynurenine, observed in the emission spectra at 470 nm. The quenching process increases up to a concentration around 5.3 mg/mL, when it saturates due to a limitation of TrpAgNP surface area/PPIX molecule. Studies on the interactions between silver nanoparticles and PPIX have become essential to understand the photophysical behavior of tissues when exposed to an environment containing metallic nanoparticles, contributing to elucidate the possible impacts that these materials may have in therapy.

Acknowledgments The authors are grateful to FAPESP (2014/06960-9) and CNPq, Brazilian funding agencies, for their financial support.

Compliance with ethical standards

Conflict of interest The authors declare that they have no conflict of interest.

References

- Austin LA, Ahmad S, Kang B, Rommel KR, Mahmoud M, Peek ME, El-Sayed MA (2015) Cytotoxic effects of cytoplasmic-targeted and nuclear-targeted gold and silver nanoparticles in HSC-3 cells - a mechanistic study. *Toxicol in Vitro* 29:694–705
- Bae SJ, Lee DS, Berezin V, Kang U, Lee KH (2016) Multispectral autofluorescence imaging for detection of cervical lesions: a preclinical study. *J Obstet Gynaecol Res* 42:1846–1853
- Baskaran B, Muthukumarasamy A, Chidambaram S, Sugumaran A, Ramachandran K, Manimuthu TR (2017) Cytotoxic potentials of biologically fabricated platinum nanoparticles from *Streptomyces* sp. on MCF-7 breast cancer cells. *Int Nanobiotechnol* 11:241–246
- Bastus NG, Merkoci F, Piella J, Puentes V (2014) Synthesis of highly monodisperse citrate-stabilized silver nanoparticles of up to 200 nm: kinetic control and catalytic properties. *Chem Mater* 26:2836–2846
- Blanco KC, Moriyama LT, Inada NM, Salvio AG, Menezes PFC, Leite EJS, Kurachi C, Bagnato VS (2015) Fluorescence guided PDT for optimization of the outcome of skin cancer treatment. *Front Phys* 3:30
- Bravo JJ, Olson JD, Davis SC, Roberts DW, Paulsen KD, Kanick SC (2017) Hyperspectral data processing improves PpIX contrast during fluorescence guided surgery of human brain tumors. *Sci Rep* 7:9455
- Courrol LC, Silva FR d O, Gomes L (2007) A simple method to synthesize silver nanoparticles by photo-reduction. *Colloids Surf A Physicochem Eng Asp* 305:54–57
- de Matos RA, Courrol LC (2017) Biocompatible silver nanoparticles prepared with amino acids and a green method. *Amino Acids* 49:379–388
- de Oliveira Silva FR, Bellini MH, Nabeshima CT, Schor N, Vieira ND Jr, Courrol LC (2011) Enhancement of blood porphyrin emission intensity with aminolevulinic acid administration: a new concept for photodynamic diagnosis of early prostate cancer. *Photodiagn Photodyn Ther* 8:7–13
- Desai R, Mankad V, Gupta SK, Jha PK (2012) Size distribution of silver nanoparticles: UV-visible spectroscopic assessment. *Nanosci Nanotechnol Lett* 4(4):30–34
- Devi L, Das S, Mandal AB (2014) Impact of surface functionalization of AgNPs on binding and conformational change of hemoglobin (Hb) and hemolytic behavior. *J Phys Chem C* 118:29739–29749
- Durán M, Silveira CP, Durán N (2015) Catalytic role of traditional enzymes for biosynthesis of biogenic metallic nanoparticles: a mini-review. *IET Nanobiotechnol* 9:314–323
- Feliu N, Huhn J, Zyuzin MV, Ashraf S, Valdeperez D, Masood A, Said AH, Escudero A, Pelaz B, Gonzalez E, Duarte MAC, Roy S, Chakraborty I, Lim ML, Sjoqvist S, Jungebluth P, Parak WJ (2016) Quantitative uptake of colloidal particles by cell cultures. *Sci Total Environ* 568:819–828
- Feuerstein T, Berkovitch-Luria G, Nudelman A, Rephaeli A, Malik Z (2011) Modulating ALA-PDT efficacy of mutlidrug resistant MCF-7 breast cancer cells using ALA prodrug. *Photochem Photobiol Sci* 10:1926–1933
- Giantsoudi D, Adams J, MacDonald SM, Paganetti H (2017) Proton treatment techniques for posterior Fossa tumors: consequences for linear energy transfer and dose-volume parameters for the brainstem and organs at risk. *Int J Radiat Oncol Biol Phys* 97:401–410
- Gottesman R, Shukla S, Perkas N, Solovyov LA, Nitzan Y, Gedanken A (2011) Sonochemical coating of paper by microbicidal silver nanoparticles. *Langmuir* 27:720–726
- Han Y and Chen J J Z 2013 Oxidative stress induces mitochondrial DNA damage and cytotoxicity through independent mechanisms in human cancer cells. *Biomed Res Int*
- Horikoshi S, Abe H, Torigoe K, Abe M, Serpone N (2010) Access to small size distributions of nanoparticles by microwave-assisted synthesis. Formation of ag nanoparticles in aqueous carboxymethylcellulose solutions in batch and continuous-flow reactors. *Nanoscale* 2:1441–1447
- Huntosova V, Gerelli E, Zellweger M, Wagnieres G (2016) Effect of PpIX photoproducts formation on pO(2) measurement by time-resolved delayed fluorescence spectroscopy of PpIX in solution and in vivo. *J Photochem Photobiol B Biol* 164:49–56

- Imahori H, Fujimoto A, Kang S, Hotta H, Yoshida K, Umeiyama T, Matano Y, Isoda S, Isosomppi M, Tkachenko NV, Lemmetyinen H (2005) Host– guest interactions in the supramolecular incorporation of fullerenes into tailored holes on porphyrin- modified gold nanoparticles in molecular photovoltaics. *Chem Eur J* 11:7265–7275
- Kamat PV (2002) Photophysical, photochemical and photocatalytic aspects of metal nanoparticles. *J Phys Chem B* 106: 7729–7744
- Kettler K, Veltman K, van de Meent D, van Wezel A, Hendriks AJ (2014) Cellular uptake of nanoparticles as determined by particle properties, experimental conditions, and cell type. *Environ Toxicol Chem* 33:481–492
- Lesniak WG, Jyoti A, Mishra MK, Louissaint N, Romero R, Chugani DC, Kannan S, Kannan RM (2013) Concurrent quantification of tryptophan and its major metabolites. *Anal Biochem* 443:222–231
- Li L, Chen Y, Wang XB, Feng XL, Wang P, Liu QH (2014) Comparison of protoporphyrin IX produced cell proliferation inhibition between human breast cancer MCF-7 and MDA-MB-231 cells. *Pharmazie* 69:621–628
- Linnert T, Mulvaney P, Henglein A (1993) Surface-chemistry of colloidal silver - surface-plasmon damping by chemisorbed I-, SH-, And C6H5S. *J Phys Chem* 97:679–682
- Mansfield JR, Gossage KW, Hoyt CC, Levenson RM (2005) Autofluorescence removal, multiplexing, and automated analysis methods for in-vivo fluorescence imaging. *J Biomed Opt* 10:041207
- Millon SR, Ostrander JH, Yazdanfar S, Brown JQ, Bender JE, Rajeha A, Ramanujam N (2010) Preferential accumulation of 5-aminolevulinic acid-induced protoporphyrin IX in breast cancer: a comprehensive study on six breast cell lines with varying phenotypes. *J Biomed Opt* 15:018002
- Mukha I, Vityuk N, Sevrynovska O, Eremenko A, Smirnova N (2016) The pH-dependent Structure and properties of au and ag nanoparticles produced by tryptophan reduction. *Nanoscale Res Lett* 11:101
- Murphy S, Huang L, Kamat PV (2011) Charge- transfer complexation and excited- state interactions in porphyrin- silver nanoparticle hybrid structures. *J Phys Chem C* 115:22761–22769
- Namikawa T, Yatabe T, Inoue K, Shuin T, Hanazaki K (2015) Clinical applications of 5-aminolevulinic acid-mediated fluorescence for gastric cancer. *World J Gastroenterol* 21:8769–8775
- Navarro JRG, Werts MHV (2013) Resonant light scattering spectroscopy of gold, silver and gold-silver alloy nanoparticles and optical detection in microfluidic channels. *Analyst* 138: 583–592
- Rai MK, Deshmukh SD, Ingle AP, Gade AK (2012) Silver nanoparticles: the powerful nanoweapon against multidrug-resistant bacteria. *J Appl Microbiol* 112:841–852
- Sanna V, Pala N, Sechi M (2014) Targeted therapy using nanotechnology: focus on cancer. *Int J Nanomedicine* 9:467–483
- Satapathy SR, Mohapatra P, Preet R, Das D, Sarkar B, Choudhuri T, Wyatt MD, Kundu CN (2013) Silver-based nanoparticles induce apoptosis in human colon cancer cells mediated through p53. *Nanomedicine* 8:1307–1322
- Satapathy SR, Mohapatra P, Preet R, Das D, Nayak A, Das S, Choudhuri T, Wyatt MD, Kundu CN (2014) Silver-based nanoparticles induce apoptosis in human colon cancer cells mediated through p53. *Anticancer Res* 34:6155–6156
- Shang L, Nienhaus K, Nienhaus GU (2014) Engineered nanoparticles interacting with cells: size matters. *J Nanobiotechnol* 12:5
- Shmarakov IO, Mukha IP, Karavan VV, Chunikhin OY, Marchenko MM, Smirnova NP, Eremenko AM (2014) Tryptophan- assisted synthesis reduces bimetallic gold/ silver nanoparticle cytotoxicity and improves biological activity. *Nanobiomedicine* 1:6
- Silva FRO, Nabeshima CT, Bellini MH, Schor N, Vieira ND Jr, Courrol LC (2013) Study of ProtoPorphyrin IX elimination by body excreta: a new noninvasive Cancer diagnostic method? *J Fluoresc* 23:131–135
- Song H, Park H, Kim YS, Kim KD, Lee HK, Cho DH, Yang JW, Hur DY (2011) L-kynurenine-induced apoptosis in human NK cells is mediated by reactive oxygen species. *Int Immunopharmacol* 11:932–938
- Sunar U, Rohrbach DJ, Morgan J, Zeitouni N, Henderson BW (2013) Quantification of PpIX concentration in basal cell carcinoma and squamous cell carcinoma models using spatial frequency domain imaging. *Biomed Opt Express* 4:531–537
- Suresh AK, Pelletier DA, Wang W, Morrell-Falvey JL, Gu BH, Doktycz MJ (2012) Cytotoxicity induced by engineered silver Nanocrystallites is dependent on surface coatings and cell types. *Langmuir* 28:2727–2735
- Sweet MJ, Chesser A, Singleton I (2012) Review: metal-based nanoparticles; size, function, and areas for advancement in applied microbiology. *Adv Appl Microbiol* 80(80):113–142
- Tang Y, Shen YF, Huang LB, Lv GJ, Lei CH, Fan XY, Lin FX, Zhang YX, Wu LH, Yang YJ (2015) In vitro cytotoxicity of gold nanorods in A549 cells. *Environ Toxicol Pharmacol* 39: 871–878
- Thompson CM, Sonawane B, Barton HA, DeWoskin RS, Lipscomb JC, Schlosser P, Chiu WA, Krishnan K (2008) Approaches for applications of physiologically based pharmacokinetic models in risk assessment. *J Toxicol Environ Health B Crit Rev* 11:519–547
- Tomita RJ, de Matos RA, Vallim MA, Courrol LC (2014) A simple and effective method to synthesize fluorescent nanoparticles using tryptophan and light and their lethal effect against bacteria. *J Photochem Photobiol B Biol* 140:157–162
- Valko M, Rhodes CJ, Moncol J, Izakovic M, Mazur M (2006) Free radicals, metals and antioxidants in oxidative stress-induced cancer. *Chem Biol Interact* 160:1–40
- Weis BK, Balshawl D, Barr JR, Brown D, Ellisman M, Liow P, Omenn G, Potter JD, Smith MT, Sohn L, Suk WA, Sumner S, Swenberg J, Walt DR, Watkins S, Thompson C, Wilson SH (2005) Personalized exposure assessment: promising approaches for human environmental health research. *Environ Health Perspect* 113:840–848
- Xin LL, Wang JS, Fan GQ, Che BZ, Wu YH, Guo SF, Tong J (2016) Oxidative stress and mitochondrial injury-mediated cytotoxicity induced by silver nanoparticles in human A549 and HepG2 cells. *Environ Toxicol* 31:1691–1699
- Yang X, Palasuberniam P, Kraus D, Chen B (2015) Aminolevulinic acid-based tumor detection and therapy:

- molecular mechanisms and strategies for enhancement. *Int J Mol Sci* 16:25865–25880
- Yen H-J, Hsu S-h, Tsai C-L (2009) Cytotoxicity and immunological response of gold and silver nanoparticles of different sizes. *Small* 5:1553–1561
- Zhang XF, Liu ZG, Shen W, Gurunathan S (2016) Silver nanoparticles: synthesis, characterization, properties, applications, and therapeutic approaches. *Int J Mol Sci* 17(34)
- Zhou YM, Liang XL, Dai ZF (2016) Porphyrin-loaded nanoparticles for cancer theranostics. *Nanoscale* 8:12394–12405